J. Indian Chem. Soc.,
Vol. 92, December 2015, pp. 1981-1991

Palladium(II) complexes of a redox-active *o*-aminophenolate-based ONSN ligand. Proof-of-concept of hemilability in reactivity with PPh_3 providing ONNP and ONSP coordination†

Akram Ali, Arunava Sengupta and Rabindranath Mukherjee*

Department of Chemistry, Indian Institute of Technology Kanpur, Kanpur-208 016, Uttar Pradesh, India and

Department of Chemical Sciences, Indian Institute of Science Education and Research Kolkata, Mohanpur-741 246, West Bengal, India

E-mail : rnm@iitk.ac.in, rnm@iiserkol.ac.in

Abstract : Using a potentially tetradentate redox-active *o*-aminophenol-based ligand, H_2L = 2-(2-ethylthio)pyridine-anilino-4,6-di-*tert*-butylphenol, we recently reported synthesis and structural characterization of three *O*,*N*,*S*,*N*-coordinated square-planar Pd^{II} complexes, green $[Pd^{II}\{(L^{AP})^{2-}\}]$ 1 (S = 0), red $[Pd^{II}\{(L^{ISQ})^{\bullet-}\}][PF_6]\cdot CH_2Cl_2$ 2 (S = 1/2), and dark green $[Pd^{II}\{(L^{IBQ})^0\}][BF_4]_2\cdot 2CH_2Cl_2$ 3 (S = 0), where the coordinated ligand is present as dianionic $(L^{AP})^{2-}$, monoanionic *o*-iminobenzosemiquinonate(1–) π-radical (S_{rad} = 1/2) $(L^{ISQ})^{\bullet-}$, and neutral *o*-iminobenzoquinone $(L^{IBQ})^0$ redox level. Reaction of complexes 1 and 2 with PPh_3 afforded isolation of two crystalline complexes, dark green $[Pd^{II}\{(L^{Ap})^{2-}\}(PPh_3)]$ 4 and red $[Pd^{II}\{(L^{ISQ})^{\bullet-}\}(PPh_3)][PF_6]\cdot CH_2Cl_2$ 5. X-Ray structure determination of complex 5 at 100(2) K revealed $Pd^{II}ON_2P$ coordination environment (A. Ali, S. K. Barman and R. Mukherjee, *Inorg. Chem.*, 2015, 54, 5182–5194). The present work reports X-ray structure determination of complex 4, which revealed $Pd^{II}ONSP$ coordination environment. Notably, the ethylpyridine arm remains non-coordinated. When examined by cyclic voltammetry (CV), complex 4 exhibits two quasireversible oxidative responses at $E_{1/2}$ = 0.08 (peak-to-peak separation, ΔE_p = 140 mV) and 0.65 V (ΔE_p = 150 mV) vs SCE (saturated calomel electrode). Both the redox processes are supposedly ligand-based. Absorption spectral property of complex 4 has also been investigated. Density Functional Theory (DFT) calculations at B3LYP-level of theory adequately describe the electronic structure of complex 4, containing a spin-paired d^8 Pd^{II} ion. Time-Dependent (TD)-DFT calculation shed light on the origin of observed spectral absorptions for complex 4.

Keywords : Redox-active tetradentate ligand, square-planar Pd^{II} complexes, crystal structure, hemilability, redox and absorption spectral properties, DFT and TD-DFT calculations.

Introduction

Generation of ligand radicals can lead to interesting ligand-centered reactivity[1–3], with the mechanism of galactose oxidase[4] serving as an inspiration for synthetic inorganic chemists. The design of metal complexes to catalyze multielectron reactions usually relies on one or more transition-metal ions capable of two-electron changes in a formal oxidation state. An alternative strategy to multielectron chemistry employs redox-active ligands, as reservoirs of electrons to supply oxidizing or reducing equivalents for bond-breaking and bond-making reactions at coordinatively unsaturated metal complexes. From this perspective metal complexes of hemilabile redox-active chelating ligands play important roles in catalysis.

Redox-active ligands profoundly influence the electronic structural properties of the resulting complexes[5]. As a part of our continued activity in this area of research[6], recently we reported[6b] the synthesis of three mononuclear square-planar palladium(II) complexes of redox-active tetradentate ligand H_2L (Fig. 1) $[Pd^{II}\{(L^{AP})^{2-}\}]$ (S = 0) **1** with a closed-shell *o*-amidophenolato(2–) dianion $(L^{AP})^{2-}$ and $[Pd^{II}\{(L^{ISQ})^{\bullet-}\}][PF_6]\cdot CH_2Cl_2$ (S = 1/2) **2** and $[Pd^{II}\{(L^{IBQ})^0\}][BF_4]_2\cdot 2CH_2Cl_2$ (S = 0) **3**, containing an *o*-iminobenzosemiquinonate(1–) $(L^{ISQ})^{\bullet-}$ π-radical and a closed-shell *o*-iminobenzoquinone $(L^{IBQ})^0$. The complexes belong to

†In honour of Professor Animesh Chakravorty on the occasion of his 80th birth anniversary.

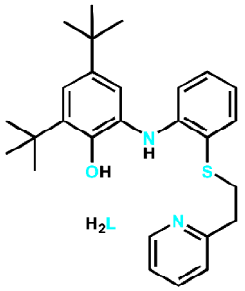

Fig. 1. The ligand H_2L.

a family of three-member ligand-based electron-transfer series. The reactivity potential of complexes **1** and **2** toward an externally added ligand PPh_3 was investigated. Coordination flexibility was identified in the isolation of complexes $[Pd(L)(PPh_3)]$ **4** and $[Pd^{II}\{(L^{ISQ})^{\bullet-}\}(PPh_3)][PF_6]\cdot CH_2Cl_2$ (S = 1/2) **5** (Fig. 2). Crystal structure analysis of complexes **1–3** and **5** at 100(2) K established unambiguously the oxidation-level of the coordinated redox-active ligand. DFT calculations provided insight into the electronic structure of the complexes. The observed switch-over of coordination site flexibility (*hemilability*)[31,3o] in the reactions of PPh_3 with complexes **1** and **2** points toward a substrate-binding capability, expected during a catalytic reaction. In this report we present structural characterization of complex **4** at 100(2) K, along with its absorption spectroscopic and redox properties. DFT and TD-DFT calculations on complex **4** have allowed us to correctly assign the electronic structure of the complex and rationalization of observed absorption spectral transitions, respectively.

Experimental

Materials :

All reagents were obtained from commercial sources and used as received. Solvents were dried/purified as reported previously[6]. Tetra-*n*-butylammonium perchlorate (TBAP) was prepared and purified as before[6]. The ligand H_2L was synthesized following a reported procedure[6b].

Synthesis of complex :

[Pd(L)(PPh$_3$)] (**4**) : To a solution of $[Pd\{(L^{AP})^{2-}\}]$ **1** (0.050 g, 0.09 mmol) in CH_2Cl_2 (10 mL), solid PPh_3 (0.024 g, 0.09 mmol) was added. The colour of the solution immediately changed from green to dark green. After stirring for 2 h at 298 K, the volume of the solution was reduced to ~2 mL, and *n*-hexane (10 mL) was added. This resulted in the separation of a dark green solid, which was collected by filtration, washed with *n*-hexane, and dried in vacuum. Yield : 0.055 g, ~75%; Anal. Calcd.

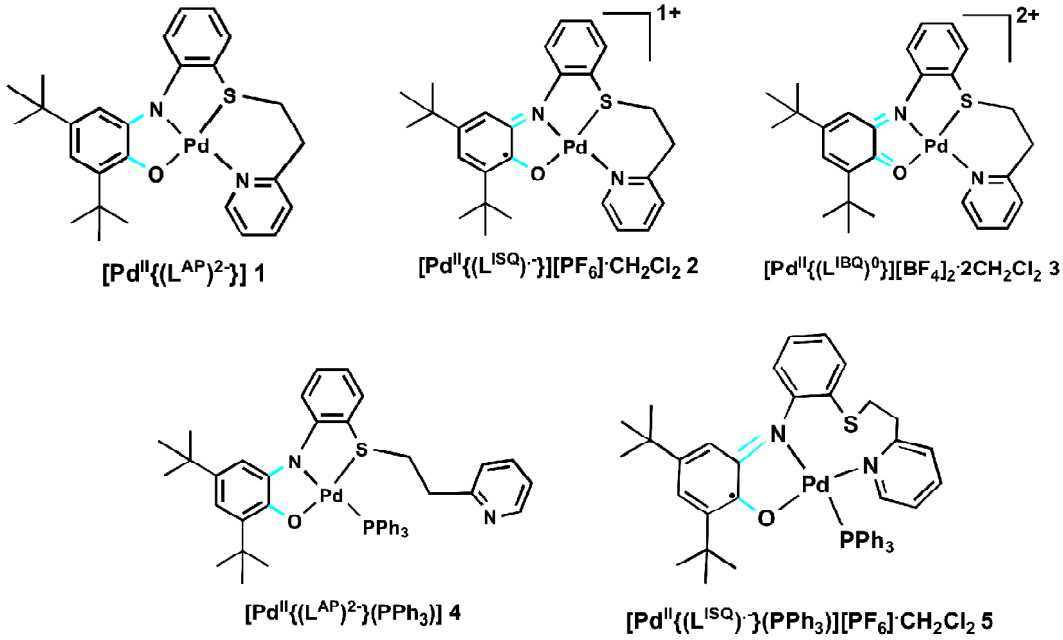

Fig. 2. Schematic representations of the complexes **1**–**5**.

for $C_{45}H_{47}N_2OPSPd$ (**4**) : C, 67.47; H, 5.87; N, 3.49. Found : C, 66.75; H, 5.94; N, 3.45%; ^{1}H NMR ($CDCl_3$, 500 MHz) δ (ppm) : 1.28 (9H, s, *tert*-butyl), 1.46 (9H, s, *tert*-butyl), 3.03 (2H, m, -CH_2-), 3.23 (2H, m, -CH_2-), 6.75 (1H, s, Ph-H_{11}), 6.94 (1H, t, *J* 7.45 Hz, Ph-H_8), 7.02 (2H, m, Ph-H_{10} and Ph-H_{12}), 7.07 (1H, d, Ph-H_7), 7.17 (1H, t, Ph-H_9), 7.35–7.45 (2H, m, Ph-H_{17} and Py-H_4), 7.54 (1H, t, *J* 7.45 Hz, Py-H_2), 7.66 (1H, t, *J* 7.45 Hz, Ph-H_{16}), 7.78–7.74 (2H, m, Ph-H_{15} and Py-H_3), 8.35 (1H, d, *J* 5.75 Hz, Py-H_1).

Physical measurements :

Elemental analysis was obtained using Thermo Quest EA1110 CHNS-O, Italy. UV-Vis spectra were recorded at 298 K using an Agilent 8453 diode-array spectrophotometer. ^{1}H NMR spectrum ($CDCl_3$) was obtained on a JEOL JNM LA 500 (500 MHz) spectrometer. Chemical shifts are reported in ppm referenced to TMS. ESI-MS spectra were recorded on a Waters-HAB213 spectrometer.

Cyclic voltammetric (CV) experiment was performed at 298 K by using CH Instruments Electrochemical Analyzer/Workstation model 600B series. The cell contained a Beckman M-39273 platinum-inlay working electrode, a Pt wire auxiliary electrode, and a saturated calomel electrode (SCE), as reference electrode. Details of the cell configuration are as described before[6]. The solutions were ~1.0 mM in complex and 0.1 *M* in supporting electrolyte, TBAP.

Under our experimental conditions, the $E_{1/2}$ and peak-to-peak separation (ΔE_p) values in CH_2Cl_2 for $[Fe^{III}(\eta^5\text{-}C_5H_5)_2]^+/[Fe^{II}(\eta^5\text{-}C_5H_5)_2]$ (Fc^+/Fc) couple were 0.49 V vs SCE and 120 mV, respectively[6].

X-Ray crystallography :

Vapour-diffusion of *n*-pentane to a CH_2Cl_2 solution of the complex $[Pd\{(L^{AP})^{2-}\}(PPh_3)]$ **4** afforded single-crystals of composition $[Pd(L)(PPh_3)]\cdot 0.5H_2O$ (**4**·0.5H_2O) suitable for X-ray diffraction. A single-crystal of suitable dimension was used for data collection. Diffraction intensities were collected on a Bruker SMART APEX CCD diffractometer, with graphite-monochromated Mo Kα (λ = 0.71073 Å) radiation at 100(2) K. The data were corrected for absorption. The structure was solved by SIR-97, expanded by Fourier-difference syntheses, and refined with SHELXL-97 incorporated in WinGX 1.64 crystallographic package[7]. The positions of the hydrogen atoms were calculated by assuming ideal geometries, but not refined. All non-hydrogen atoms were refined with anisotropic thermal parameters by full-matrix least-squares procedures on F^2. The asymmetric unit contains two molecules of $[Pd(L)(PPh_3)]$ and a water molecule as solvent of crystallization. The hydrogen atoms of such a H_2O molecule could not be fixed. Selected crystal data and data collection parameters are given in Table 1.

Table 1. Crystallographic data for $[Pd\{(L^{AP})^{2-}\}(PPh_3)]\cdot 0.5H_2O$ (**4**·0.5H_2O)

Empirical formula	$C_{45}H_{47}N_2O_{1.5}PSPd$
Formula mass	809.28
Crystal system	Triclinic
Space group	P-1
a (Å)	10.7964(5)
b (Å)	19.0625(10)
c (Å)	19.5925(9)
α (deg)	86.5820(10)
β (deg)	79.3230(10)
γ (deg)	89.9390(10)
V (Å^3)	3955.2(3)
Z	4
$D_{Calcd.}$ (mg m^{-3})	1.359
T (K)	100(2)
μ (mm^{-1})	0.600
$R_1{}^a$	0.0552
$wR_2{}^b$	0.1261
GOF	0.942

$^aR_1 = \Sigma||F_o| - |F_c||/\Sigma|F_o|$. $^bwR_2 = \{\Sigma[w(|F_o|^2 - |F_c|^2)^2]/\Sigma[w(|F_o|^2)^2]\}^{1/2}$.

Computational details :

All DFT calculations were performed using the Gaussian 09 program[8] with B3LYP functional[9]. Hay and Wadt basis set LANL2DZ with pseudopotential[10] was employed for palladium. Triple-ζ quality basis sets (TZVP)[11] were used for sulfur, oxygen, and nitrogen while the SVP basis set[12] was used for all other atoms. TD-DFT calculations were done employing the B3LYP functional and the polarizable continuum model, CPCM (CH_2Cl_2 as solvent)[13]. TD-DFT-derived electronic spectra were plotted using GaussSum[14]. Corresponding orbitals were made using Chemcraft[15] Visualization program.

Results and discussion

Synthesis and characterization :

The *N*-substituted *o*-aminophenolates as ligands[16,17] have been popularized primarily by Wieghardt *et al.*[18]. The aminophenols are easily prepared and derivatized. For example, 3,5-di-*tert*-butylcatechol reacts with primary aromatic amines to give a range of aminophenols. Under a dinitrogen atmosphere, stoichiometric reaction of 3,5-di-*tert*-butylcatechol with ([2′-aminophenylthio]ethyl)-pyridine[19] in the presence of Et_3N in *n*-heptane led to the isolation of ligand H_2L[6b].

The synthesis and characterization of three Pd^{II} complexes with the *o*-aminophenolate-based tetradentate ligand coordinated in three oxidation-levels $[Pd^{II}\{(L^{AP})^{2-}\}]$ **1**, $[Pd^{II}\{(L^{ISQ})^{\bullet-}\}][PF_6]\cdot CH_2Cl_2$ **2**, and $[Pd^{II}\{(L^{IBQ})^{0}\}]-[BF_4]_2\cdot 2CH_2Cl_2$ **3** have recently been reported[6b]. Reactivity of complexes **1** and **2** with PPh_3 led to isolation of two more complexes $[Pd^{II}\{(L^{AP})^{2-}\}(PPh_3)]$ **4** and $[Pd^{II}\{(L^{ISQ})^{\bullet-}\}(PPh_3)][PF_6]\cdot CH_2Cl_2$ **5**, showing proof-of-concept of *hemilability*[3l,3o]. Complexes **1**–**3** and **5** were structurally characterized. Complex **5** was shown to assume a square-planar geometry with coordination by *O*,*N* from the *o*-aminophenolate part, ethylpyridyl *N*, and PPh_3[6b]. Thus at the expense of PPh_3 coordination, thioether *S* remained non-coordinated. It was demonstrated that in complex **4** *O*,*N* from the *o*-aminophenolate part, thioether *S*, and PPh_3 are coordinated to the Pd^{II} ion. Thus pyridine of ethylpyridine arm remained non-coordinated (Fig. 3). Elemental analysis and ESI-MS data (Fig. 4) attested the composition of complex **4**. However, the crystal structure of **4** was not reported in earlier publication[6b].

Metal complexes of *o*-aminophenolates provide an archetype for understanding the ligand-based redox activity. Three basic oxidation-levels dominate the coordination chemistry of *o*-aminophenolate ligands bound to metal ions, the closed-shell diamagnetic dianionic aminophenolate/amidophenolate form $(L^{AP})^{2-}$, the open-shell paramagnetic monoanionic *o*-iminosemiquinonate(1–) π-radical $(L^{ISQ})^{\bullet-}$ (S_{rad} = 1/2) form, and the closed-shell diamagnetic neutral *o*-iminobenzoquinone $(L^{IBQ})^0$ form (Scheme 1).

In order to authenticate the structure of complex **4**, single-crystal X-ray crystallographic analysis has been done. Structural analysis reveals that the asymmetric unit contains crystallographically independent two independent molecules of the palladium complex and a water molecule. The metal-ligand bonding parameters are closely similar and hence the structure of one of the molecules is

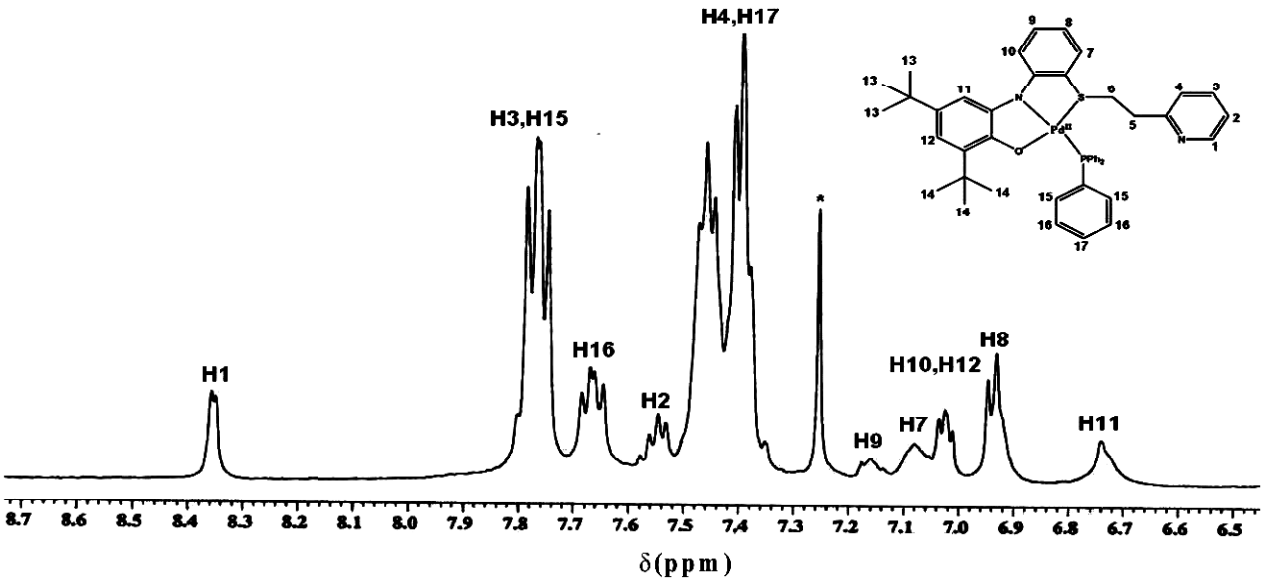

Fig. 3. ^1H NMR spectrum (500 MHz, $CDCl_3$) of $[Pd\{(L^{AP})^{2-}\}(PPh_3)]$ **4**. Peaks denoted by * is due to $CHCl_3$. Only expanded 6.5–8.7 ppm region is displayed (ONSP coordination).

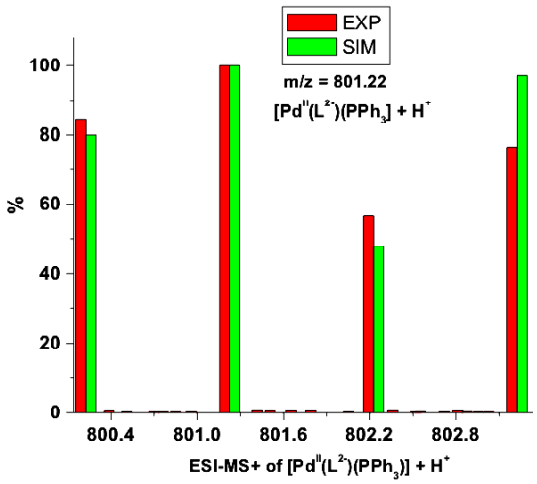

Fig. 4. Positive-ion ESI-MS of $[Pd^{II}\{L^{AP})^{2-}\}(PPh_3)]$ **4**.

displayed in Fig. 5. Selected metric parameters for both the molecules are listed in Table 2. The structure shows that the potentially tetradentate ligand is coordinated to the palladium as a tridentate ligand, utilizing its phenolate *O*, amido/iminate *N*, and the thioether *S*. It is interesting to note that in spite of having the pyridine as a potential donor site, the *o*-aminophenolate ligand L(2–) has not used it for coordination. Instead, a triphenylphosphine is coordinated to the metal centre completing four-coordination.

The metal coordination environment in complex $[Pd(L)(PPh_3)]\cdot 0.5H_2O$ (**4**·$0.5H_2O$) is identified by Pd-O1(phenolate), Pd-N1(amidate/iminate), Pd-S1(thioether) and Pd-P1(PPh_3) distances, respectively : 2.007(3)

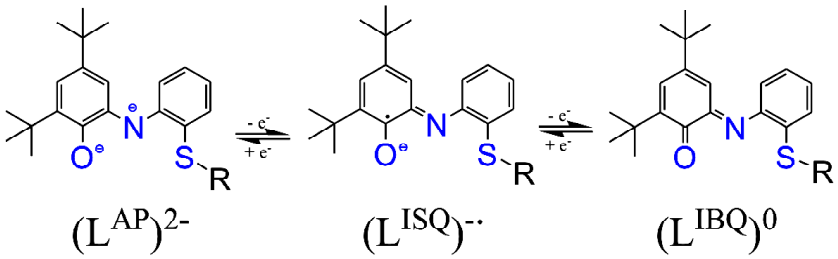

Scheme 1. The geometric and electronic features (redox-levels) observed for L(2–).

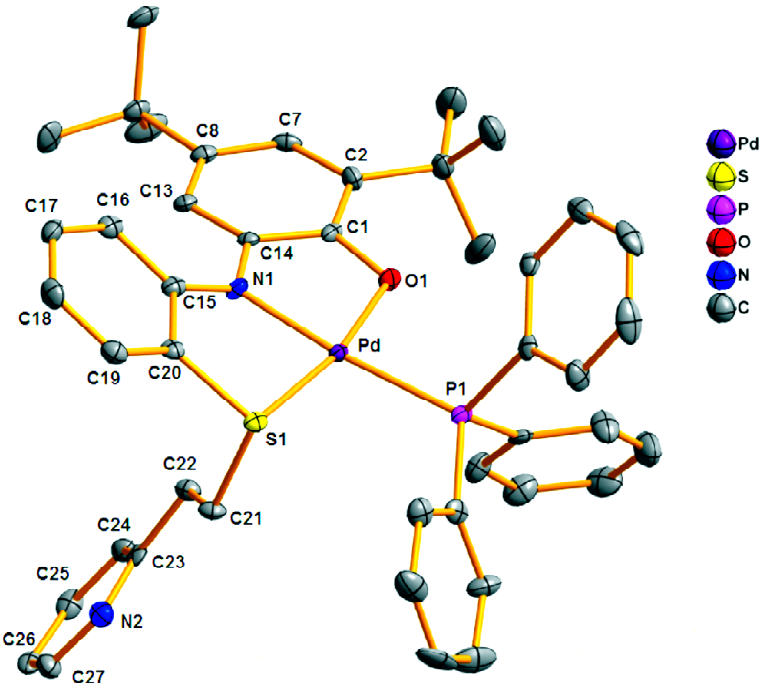

Fig. 5. Perspective view of the metal coordination environment in $[Pd(L)(PPh_3)]\cdot 0.5H_2O$ (**4**·$0.5H_2O$). Ellipsoids are drawn at 50% probability. Hydrogen atoms and solvent molecules have been left out for clarity.

Table 2. Selected bond lengths (Å) and bond angles (deg) in $[Pd(L)(PPh_3)]\cdot 0.5H_2O$ ($\mathbf{4}\cdot 0.5H_2O$)

Bond distances (Å)	
Pd-N1	1.989(4) [1.987(4)]
Pd-P1	2.2867(13) [2.2777(13)]
Pd-O1	2.007(3) [1.999(3)]
Pd-S1	2.2707(12) [2.2665(13)]
C1-O1	1.358(6) [1.349(6)]
C14-N1	1.405(6) [1.410(6)]
C15-N1	1.366(6) [1.365(6)]
C20-S1	1.784(5) [1.784(5)]
C21-S1	1.832(5) [1.838(5)]
C23-N2	1.338(6) [1.343(7)]
C27-N2	1.331(7) [1.340(7)]
C1-C2	1.412(7)[1.414(7)]
C2-C7	1.398(7) [1.391(7)]
C7-C8	1.393(7) [1.391(7)]
C8-C13	1.393(7) [1.378(7)]
C13-C14	1.399(7) [1.398(7)]
C14-C1	1.403(7) [1.417(7)]
C15-C16	1.410(7) [1.417(7)]
C16-C17	1.363(7) [1.374(7)]
C17-C18	1.406(7) [1.391(7)]
C18-C19	1.381(7) [1.378(7)]
C19-C20	1.371(7) [1.378(7)]
C20-C15	1.427(7) [1.418(7)]
C21-C22	1.515(7) [1.519(7)]
C22-C23	1.505(7) [1.509(7)]
C23-C24	1.395(7) [1.388(7)]
C24-C25	1.391(7) [1.381(7)]
C25-C26	1.373(8) [1.381(7)]
C26-C27	1.380(7) [1.375(7)]
Bond angles (deg)	
N1-Pd-O1	82.78(15) [83.20(15)]
N1-Pd-P1	175.84(12) [174.23(13)]
O1-Pd-P1	94.59(10) [92.25(10)]
N1-Pd-S1	84.88(12) [84.77(12)]
O1-Pd-S1	167.59(10) [167.97(10)]
P1-Pd-S1	97.66(5) [99.77(5)]

[1.999(3)], 1.989(4) [1.987(4)], 2.2707(12) [2.2665(13)], and 2.2867(13) [2.2777(13)] Å. In going from complex **1** (the Pd-O1, Pd-N1, Pd-S1, and Pd-N2(pyridine) distances are 2.004(4), 1.957(4), 2.198(2) and 2.075(4) Å, respectively) to complex $[Pd(L)(PPh_3)]\cdot 0.5H_2O$ ($\mathbf{4}\cdot 0.5H_2O$), the Pd-O1 distance remains almost unchanged. However, the Pd-N1 and Pd-S distances increase by ~0.03 and ~0.07 Å, respectively. Replacing pyridine by triphenylphosphine brings about an increase of the metal-ligand distance by ~0.2 Å. The Pd-N1 distance is the shortest and the Pd-P1 distance is the longest. Comparing the Pd-O1 and Pd-N1 bond distances in complex **1** and complex $\mathbf{4}\cdot 0.5H_2O$, it is obvious that the palladium ion in complex $\mathbf{4}\cdot 0.5H_2O$ is present in its bivalent state. In $\mathbf{4}\cdot 0.5H_2O$, the palladium(II) ion attains a grossly planar (Table 2) ONSP coordination sphere. The spatial geometry in complex **1** and complex $\mathbf{4}\cdot 0.5H_2O$ is closely similar, the only difference is N2(pyridine) in complex **1** is replaced by P1(PPh_3) in complex $\mathbf{4}\cdot 0.5H_2O$. The geometry at the metal site is distorted from ideal square-planar geometry, as reflected in the bonding angles around the Pd^{II} center. The average carbon-carbon distance in the phenolate ring of the *o*-amidophenolate is ~1.40 Å (Table 2). This attests the presence of $(L^{AP})^{2-}$ form of L(2–) that is coordinated to the Pd^{II} ion.

To investigate the possibility of identifying metal-centered redox and/or accessibility of various ligand redox-levels, CV experiment on complex **4** was carried out. The CV in CH_2Cl_2 displays (Fig. 6) two oxidative redox processes at $E_{1/2}$ values of 0.08 V (ΔE_p = 140 mV) and 0.65 V (ΔE_p = 150 mV) vs SCE. It should be mentioned here that a similar CV behavior was observed for complex **1**[6b]. Both the oxidation processes are chemically reversible (ratio of cathodic and anodic peak current, $i_{pc}/i_{pa} \approx 1$) and electrochemically quasireversible electron-transfer reactions[6].

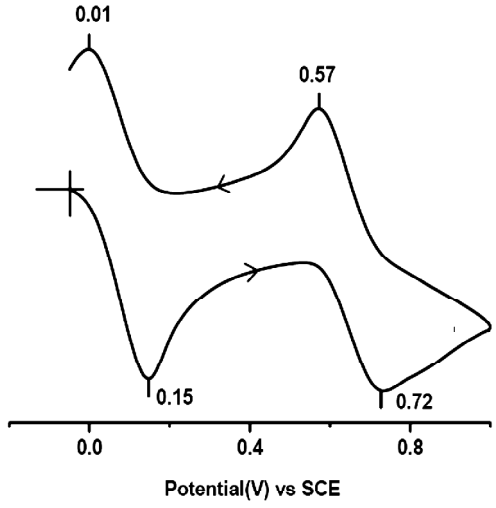

Fig. 6. Cyclic voltammogram (100 mV/s) of a 1.0 mM solution of $[Pd(L)(PPh_3)]$ in CH_2Cl_2 (0.1 *M* in TBAP) at a platinum working electrode. Indicated peak potentials are in V vs SCE.

Recently in an attempt to quantitatively determine the redox-level of redox-active ligands, Brown *et al*. proposed[20] the Metrical Oxidation States (MOSs) of ligands in complexes, based on least-squares fitting of relevant C-O, C-N, and C-C bond lengths. By this approach, using metrical parameters determined from crystal structure the empirical oxidation state of ligands can be ascertained. Using this concept the MOS of the ligand in complex **4** is calculated as –1.89 ± 0.05, which is consistent with the dianionic form (2–) of the ligand. The corresponding value for complex **1** is –1.92 ± 0.09[6b]. Using this MOS value of –1.89, the C1-O1 and C14-N1 bond distances are calculated as 1.359 and 1.396 Å, respectively, which are in excellent agreement with the X-ray determined values of 1.358(6) and 1.405(6) Å (Table 2). For complex **1** the C1-O1 and C14-N1 bond distances are calculated as 1.361 and 1.398 Å, respectively[6b]. Table 3 presents the comparison of MOS-derived calculated bond lengths and metrical parameters of relevant atoms, determined from X-ray structure.

Table 3. Comparison of X-ray determined experimental bond lengths with the calculated bond lengths (in parentheses) from Metrical Oxidation State (MOS) values of complex **4**·0.5H_2O

Bond distances (Å)	
C1-C14	1.403(7) [1.412]
C13-C14	1.399(7) [1.393]
C8-C13	1.393(7) [1.393]
C7-C8	1.393(7) [1.393]
C2-C7	1.398(7) [1.401]
C1-C2	1.412(7) [1.400]
C1-O1	1.358(6) [1.359]
C14-N1	1.405(6) [1.396]

Assignment of correct oxidation-level of the coordinated ligand and the oxidation-state of Pd in complex **4** have been done by DFT calculation at the B3LYP level of theory (see Computational Details in the Experimental section). Geometry-optimization of complex **4**·0.5H_2O (only X-ray coordinates of the molecule shown in Fig. 5 were considered) with $S = 0$ ground-state (closed-shell configuration) was computed to obtain the $[Pd^{II}\{(L^{AP}{}_{O,N,S,P})^{2-}\}(PPh_3)]$ electronic configuration (see Crystal Structure section). The calculated ground-state geometry well-reproduced that found in the crystal structure (grossly square-planar geometry of complex **4**·0.5H_2O) with the exception of the Pd^{II}-$L_{O,N,S,P}$ bond distances, which are *ca*. 0.03–0.09 Å longer than the experimental value (Table 2 and Table 4). Notably, the bond distances associated with the ligand-backbone accurately reproduce the oxidation-level of the coordinated ligand $(L^{AP})^{2-}$. Selective orbital contour plots for complex **4**·0.5H_2O are displayed in Fig. 7.

The electronic spectrum of $[Pd^{II}\{(L^{AP})^{2-}\}(PPh_3)]$ **4** in which the coordinated ligand is present as *o*-amidophenolate dianion(2–) is displayed in Fig. 8. Absorption spectral features of *o*-aminophenolate ligands are very informative with respect to the redox-level of the coordinated ligand[6b].

TD-DFT calculation was performed on complex **4** to

Table 4. X-Ray structural and DFT-optimized (in parentheses) bond-lengths of complex **4**·0.5H_2O

Pd-N1	1.989(4) [2.016]
Pd-P1	2.2867(13) [2.3716]
Pd-O1	2.007(3) [2.031]
Pd-S1	2.2707(12) [2.361]
C1-O1	1.358(6) [1.354]
C14-N1	1.405(6) [1.410]
C15-N1	1.366(6) [1.366]
C20-S1	1.784(5) [1.801]
C21-S1	1.832(5) [1.852]
C23-N2	1.338(6) [1.339]
C27-N2	1.331(7) [1.338]
C1-C2	1.412(7) [1.421]
C2-C7	1.398(7) [1.403]
C7-C8	1.393(7) [1.404]
C8-C13	1.393(7) [1.399]
C13-C14	1.399(7) [1.405]
C14-C1	1.403(7) [1.422]
C15-C16	1.410(7) [1.426]
C16-C17	1.363(7) [1.390]
C17-C18	1.406(7) [1.402]
C18-C19	1.381(7) [1.394]
C19-C20	1.371(7) [1.397]
C20-C15	1.427(7) [1.430]
C21-C22	1.515(7) [1.522]
C22-C23	1.505(7) [1.516]
C23-C24	1.395(7) [1.406]
C24-C25	1.391(7) [1.392]
C25-C26	1.373(8) [1.398]
C26-C27	1.380(7) [1.394]

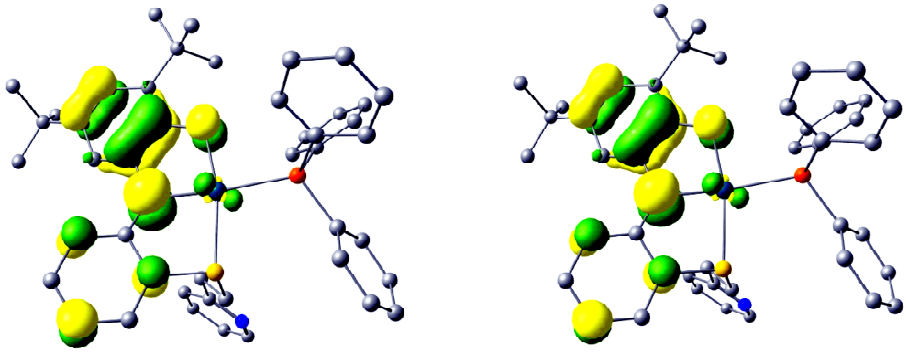

α-HOMO β-HOMO

Fig. 7. Qualitative MO diagrams for complex **4**·0.5H_2O.

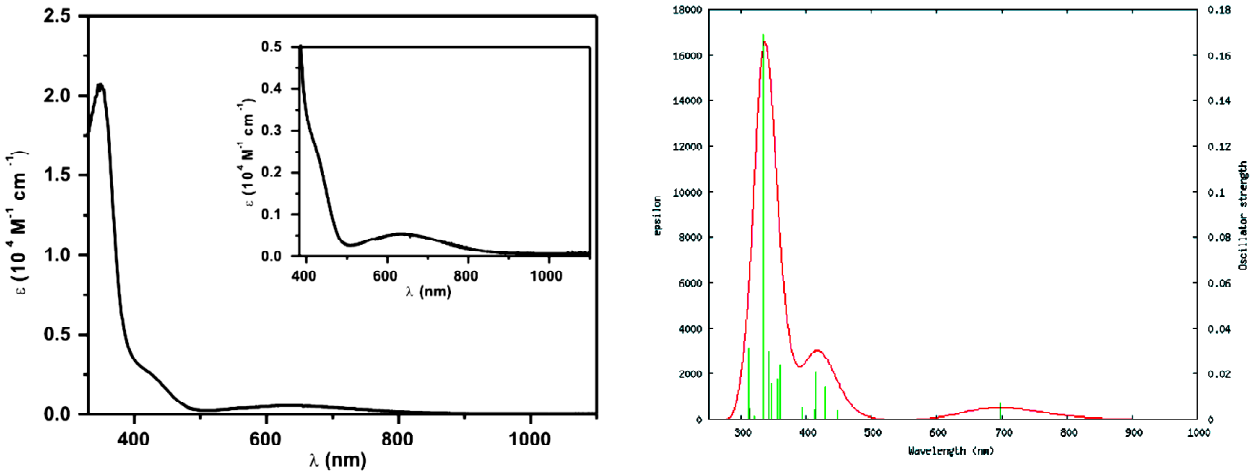

Fig. 8. (a) Electronic absorption spectrum of [Pd^{II}{(L^{AP})$^{2-}$}(PPh_3)] **4** in CH_2Cl_2. (b) TD-DFT calculated electronic spectrum of [Pd^{II}{(L^{AP})$^{2-}$}(PPh_3)] **4**.

get information about the origin of observed absorptions. In its absorption spectrum, complex **4** displays in CH_2Cl_2 characteristic absorptions in the 300–1000 nm region : 350 (20750 M^{-1} cm^{-1}), 424 (2700), 650 (575). TD-DFT calculation (Table 5) on square-planar Pd^{II} complex **4** revealed (Fig. 8) that the low-energy transition calculated at 697 nm involves excitation from (α/β)-HOMO to (α/β)-LUMO. Inspection of frontier orbitals shows that this ab-

Table 5. TD-DFT-calculated electronic transitions of [Pd^{II}{(L^{AP})$^{2-}$}(PPh_3)] complex **4**

Excitation energy (eV)	λ (nm)	*f*	Transition	Character
1.7783	697	0.007	α/β-H[~94%L]→α/β-L[~71%L] (98%)	Intraligand charge-transfer in amidophenolate, along with MLCT
2.8926	428	0.0141	α/β-H[~94%L]→α/β-L+1[~97%L] (86%)	Amidophenolate → phosphine
3.7121	334	0.1692	α/β-H[~94%L]→α/β-L+10[~93%L] (90%)	Amidophenolate → aminothioether

sorption corresponds to a combination of intraligand (amidophenolato-ligand pyridine/aminothioetherpyridine) charge-transfer (ILCT), along with ligand-to-metal charge-transfer (LMCT) transition (Fig. 9). This indicates that the experimentally observed transition at 650 nm could be a combination of ILCT and LMCT. The origin of experimentally observed transitions in 350 and 424 nm could be correlated to the TD-DFT calculated absorptions at 428 and 334 nm, which could be assigned as transitions ((α/β)-HOMO to (α/β)-LUMO + 1 and (α/β)-HOMO to (α/β)-LUMO + 10) from donor amidophenolate to the acceptor phosphine and aminothioether moiety, respectively (Fig. 9).

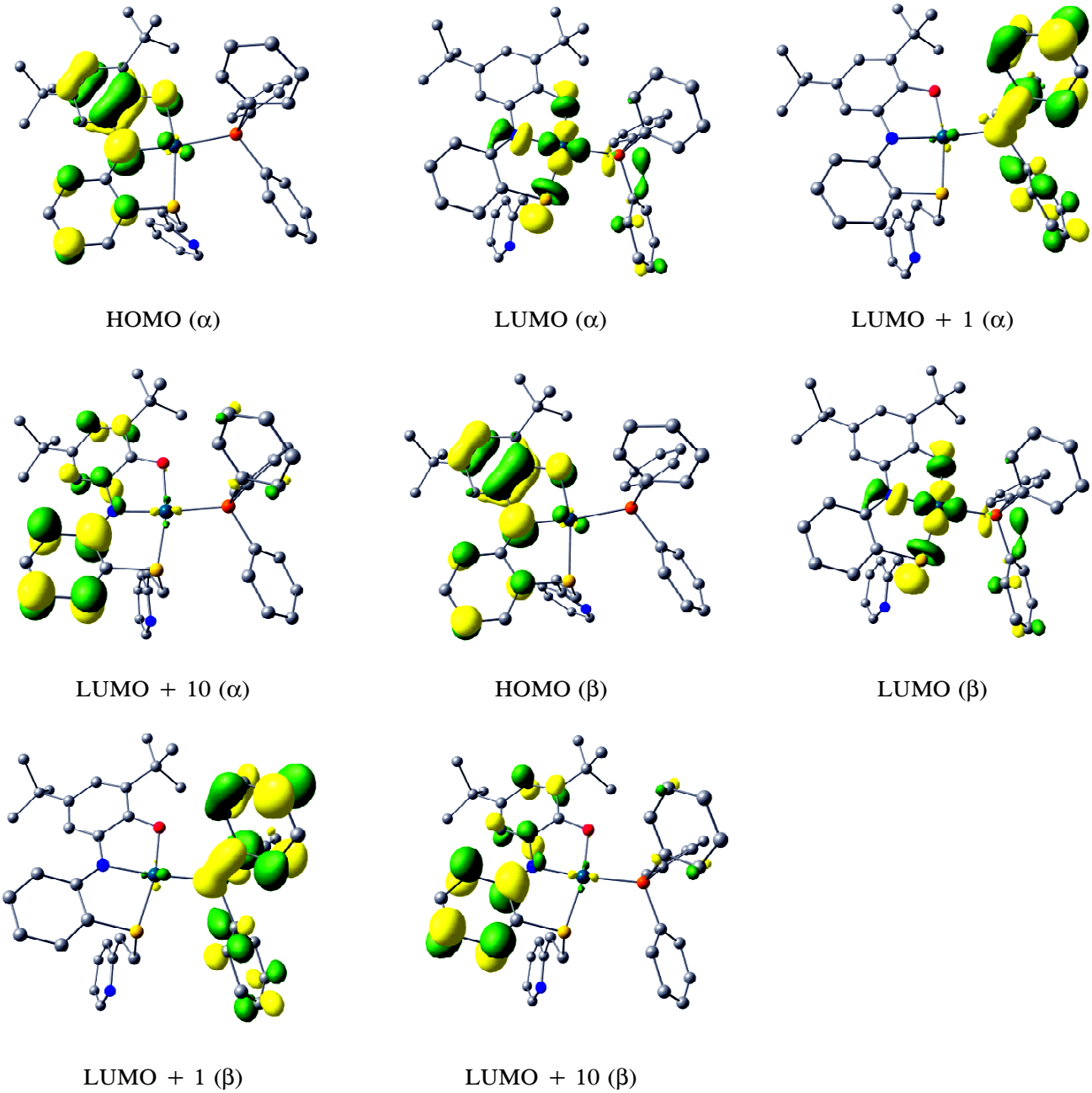

Fig. 9. Representative molecular-orbitals involved in TD-DFT transitions of $[Pd^{II}\{(L^{AP})^{2-}\}(PPh_3)]$ **4**.

Conclusion

The present study shows that when bound to palladium(II), 2-(2-ethylthio)pyridine-anilino-4,6-di-*tert*-butylphenol (L(2–)), exhibits coordination flexibility when an external ligand PPh_3 (in our work) is bound to the metal centre. However, observed coordination *hemilability* depends on the redox-level of the coordinated ligand. As for example, when PPh_3 is bound to complex **1** ($Pd^{II}(L_{O,N,S,N})$) the product complex **4** assumes $Pd^{II}(L_{O,N,S,P})$ coordination. In complexes **1** and **4** the coordinated ligand is present in its $L^{AP}(2-)$ redox-level. Similarly, when PPh_3 is bound to complex **2** ($Pd^{II}(L_{O,N,S,N})$), complex **5** assumes $Pd^{II}(L_{O,N,N,P})$ coordination. In complexes **2** and **5** the coordinated ligand is present in its $(L^{ISQ})^{\bullet-}$ π-radical redox-level. This study substantiates, through X-ray structural characterization of complex **4**, our previous claim that complex **4** has $Pd^{II}(L_{O,N,S,P})$ coordination, with eyhylpyridine arm remaining non-coordinated. The present study attests the fact that by virtue of coordination flexibility in the binding of L(2–) to Pd^{II} ion, the [Pd] complexes **1** and **2** can act as catalysts for ligand redox-driven bond-breaking/bond-making reactions. Studies on the utilization of complexes **1** and **2** for the redox-driven reactivity are currently underway and the outcome of such an investigation will be published elsewhere.

Acknowledgement

This work is supported by the Department of Science & Technology (DST), Government of India. RM sincerely thanks DST for a J. C. Bose Fellowship. AA and AS acknowledge the award of an SRF by the Council of Scientific & Industrial Research and by the University Grants Commission, Government of India, respectively.

Supplementary data

Crystallographic data of the [Pd] complex has been deposited with the Cambridge Crystallographic Data Center, CCDC numbers 1438388.

References

1. (a) V. Lyaskovskyy and B. de Bruin, *ACS Catal.*, 2012, **2**, 270; (b) V. K. K. Praneeth, M. R. Ringenberg and T. R. Ward, *Angew. Chem., Int. Ed.*, 2012, **51**, 10228; (c) O. R. Luca and R. H. Crabtree, *Chem. Soc. Rev.*, 2013, **42**, 1440; (d) D. L. J. Broere, R. Plessiusa and J. I. van der Vlugt, *Chem. Soc. Rev.*, 2015, **44**, 6886.
2. (a) D. L. J. Broere, B. de Bruin, J. N. H. Reek, M. Lutz, S. Dechert and J. I. van der Vlugt, *J. Am. Chem. Soc.*, 2014, **136**, 11574; (b) C. A. Sanz, M. J. Ferguson, R. McDonald, B. O. Patrick and R. G. Hicks, *Chem. Commun.*, 2014, **50**, 11676; (c) D. L. J. Broere, L. L. Metz, B. de Bruin, J. N. H. Reek, M. A. Siegler and J. I. van der Vlugt, *Angew. Chem., Int. Ed.*, 2015, **54**, 1516.
3. (a) P. Chaudhuri, M. Hess, J. Müller, K. Hildenbrand, E. Bill, T. Weyhermüller and K. Wieghardt, *J. Am. Chem. Soc.*, 1999, **121**, 9599; (b) K. J. Blackmore, J. W. Ziller and A. F. Heyduk, *Inorg. Chem.*, 2005, **44**, 5559; (c) M. R. Haneline and A. F. Heyduk, *J. Am. Chem. Soc.*, 2006, **128**, 8410; (d) M. R. Ringenberg, S. L. Kokatam, Z. M. Heiden and T. B. Rauchfuss, *J. Am. Chem. Soc.*, 2008, **130**, 788; (e) K. J. Blackmore, N. Lal, J. W. Ziller and A. F. Heyduk, *J. Am. Chem. Soc.*, 2008, **130**, 2728; (f) C. Mukherjee, U. Pieper, E. Bothe, V. Bachler, E. Bill, T. Weyhermüller and P. Chaudhuri, *Inorg. Chem.*, 2008, **47**, 8943; (g) A. L. Smith, L. A. Clapp, K. I. Hardcastle and J. D. Soper, *Polyhedron*, 2010, **29**, 164; (h) M. R. Ringenberg, M. J. Nilges, T. B. Rauchfuss and S. R. Wilson, *Organometallics*, 2010, **29**, 1956; (i) A. L. Smith, K. I. Hardcastle and J. D. Soper, *J. Am. Chem. Soc.*, 2010, **132**, 14358; (j) W. L. Dzik, J. I. van der Vlugt, J. N. H. Reek and B. de Bruin, *Angew. Chem., Int. Ed.*, 2011, **50**, 3356; (k) M. R. Ringenberg and T. B. Rauchfuss, *Eur. J. Inorg. Chem.*, 2012, 490; (l) R. Hübner, S. Weber, S. Strobel, B. Sarkar, S. Záliš and W. Kaim, *Organometallics*, 2011, **30**, 1414; (m) C. A. Lippert, K. I. Hardcastle and J. D. Soper, *Inorg. Chem.*, 2011, **50**, 9864; (n) F. D. Lesh, R. L. Lord, M. J. Heeg, H. B. Schlegel and C. N. Verani, *Eur. J. Inorg. Chem.*, 2012, 463; (o) M. Bubrin, D. Schweinfurth, F. Ehret, S. Záliš, H. Kvapilová, J. Fiedler, Q. Zeng, F. Hartl and W. Kaim, *Organometallics*, 2014, **33**, 4973.
4. (a) J. W. Whittaker, *Chem. Rev.*, 2003, **103**, 2347; (b) P. Chaudhuri, K. Wieghardt, T. Weyhermüller, T. K. Paine, S. Mukherjee and C. Mukherjee, *Biol. Chem.*, 2005, **386**, 1023; (c) F. Thomas, *Eur. J. Inorg. Chem.*, 2007, 2379; (d) P. J. Chirik and K. Wieghardt, *Science*, 2010, **327**, 794; (e) C. T. Lyons and T. D. P. Stack, *Coord. Chem. Rev.*, 2013, **257**, 528.
5. K. Ray, T. Petrenko, K. Wieghardt and F. Neese, *Dalton Trans.*, 2007, 1552.
6. (a) A. Rajput, A. K. Sharma, S. K. Barman, D. Koley, M. Steinert and R. Mukherjee, *Inorg. Chem.*, 2014, **53**, 36; (b) A. Ali, S. K. Barman and R. Mukherjee, *Inorg. Chem.*, 2015, **54**, 5182 and references therein.
7. L. J. Farrugia, WinGX version 1.64, An Integrated Systems of Windows Programs for the Solution, Refinement and Analysis of Single-Crystal X-ray Diffraction Data, Department of Chemistry, University of Glasgow, 2003.
8. M. J. Frisch, G. W. Trucks, H. B. Schlegel, G. E. Scuseria, M. A. Robb, J. R. Cheeseman, G. Scalmani, V. Barone, B.

Mennucci, G. A. Petersson, H. Nakatsuji, M. Caricato, X. Li, H. P. Hratchian, A. F. Izmaylov, J. Bloino, G. Zheng, J. L. Sonnenberg, M. Hada, M. Ehara, K. Toyota, R. Fukuda, J. Hasegawa, M. Ishida, T. Nakajima, Y. Honda, O. Kitao, H. Nakai, T. Vreven, J. A. Montgomery (Jr.), J. E. Peralta, F. Ogliaro, M. Bearpark, J. J. Heyd, E. Brothers, K. N. Kudin, V. N. Staroverov, R. Kobayashi, J. Normand, K. Raghavachari, A. Rendell, J. C. Burant, S. S. Iyengar, J. Tomasi, M. Cossi, N. Rega, N. J. Millam, M. Klene, J. E. Knox, J. B. Cross, V. Bakken, C. Adamo, J. Jaramillo, R. Gomperts, R. E. Stratmann, O. Yazyev, A. J. Austin, R. Cammi, C. Pomelli, J. W. Ochterski, R. L. Martin, K. Morokuma, V. G. Zakrzewski, G. A. Voth, P. Salvador, J. J. Dannenberg, S. Dapprich, A. D. Daniels, Ö. Farkas, J. B. Foresman, J. V. Ortiz, J. Cioslowski, D. J. Fox, Gaussian 09, revision B.01, Gaussian, Inc., Wallingford, CT, 2010.

9. (a) A. D. Becke, *J. Chem. Phys.*, 1993, **98**, 5648; (b) C. Lee, W. Yang and R. G. Parr, *Phys. Rev. (B)*, 1988, **37**, 785; (c) P. J. Stevens, F. J. Devlin, C. F. Chabalowski and M. Frisch, *J. Phys. Chem.*, 1994, **98**, 11623.
10. P. J. Hay and W. R. Wadt, *J. Chem. Phys.*, 1985, **82**, 270.
11. A. Schafer, C. Huber and R. Ahlrichs, *J. Chem. Phys.*, 1994, **100**, 5829.
12. A. Schafer, H. Horn and R. Ahlrichs, *J. Chem. Phys.*, 1992, **97**, 2571.
13. (a) V. Barone and M. Cossi, *J. Phys. Chem. (A)*, 1998, **102**, 1995; (b) M. Cossi and V. Barone, *J. Chem. Phys.*, 2001, **115**, 4708; (c) M. Cossi, N. Rega, G. Scalmani and V. Barone, *J. Comput. Chem.*, 2003, **24**, 669.
14. N. M. O'Boyle, A. L. Tenderholt and K. M. Langner, *J. Comput. Chem.*, 2008, **29**, 839.
15. http://www.chemcraftprog.com
16. K. P. Butin, E. K. Beloglazkina and N. V. Zyk, *Russ. Chem. Rev.*, 2005, **74**, 531.
17. A. I. Poddel'sky, V. K. Cherkasov and G. A. Abakumov, *Coord. Chem. Rev.*, 2009, **253**, 291.
18. (a) P. Chaudhuri, C. N. Verani, E. Bill, E. Bothe, T. Weyhermüller and K. Wieghardt, *J. Am. Chem. Soc.*, 2001, **123**, 2213; (b) H. Chun, C. Verani, P. Chaudhuri, E. Bothe, E. Bill, T. Weyhermüller and K. Wieghardt, *Inorg. Chem.*, 2001, **40**, 4157; (c) H. Chun, P. Chaudhuri, T. Weyhermüller and K. Wieghardt, *Inorg. Chem.*, 2002, **41**, 790; (d) D. Herebian, P. Ghosh, H. Chun, E. Bothe, T. Weyhermüller and K. Wieghardt, *Eur. J. Inorg., Chem.*, 2002, 1957; (e) V. Bachler, G. Olbrich, F. Neese and K. Wieghardt, *Inorg. Chem.*, 2002, **41**, 4179; (f) X. Sun, H. Chun, K. Hildenbrand, E. Bothe, T. Weyhermüller, F. Neese and K. Wieghardt, *Inorg. Chem.*, 2002, **41**, 4295; (g) K. S. Min, T. Weyhermüller and K. Wieghardt, *Dalton Trans.*, 2003, 1126; (h) K. S. Min, T. Weyhermüller, E. Bothe and K. Wieghardt, *Inorg. Chem.*, 2004, **43**, 2922; (i) E. Bill, E. Bothe, P. Chaudhuri, K. Chlopek, D. Herebian, S. Kokatam, K. Ray, T. Weyhermüller, F. Neese and K. Wieghardt, *Chem.-Eur. J.*, 2005, **11**, 204; (j) S. Mukherjee, T. Weyhermüller, E. Bill, K. Wieghardt and P. Chaudhuri, *Inorg. Chem.*, 2005, **44**, 7099; (k) S.-L. Kokatam, P. Chaudhuri, T. Weyhermüller and K. Wieghardt, *Dalton Trans.*, 2007, 373.
19. J. G. Gilbert, A. W. Addison and R. J. Butcher, *Inorg. Chim. Acta*, 2000, **308**, 22.
20. S. N. Brown, *Inorg. Chem.*, 2012, **51**, 1251.

1992